Morphological Study on Thermal Shrinkage and Dimensional Stability Associated with Oriented Poly(lactic acid)

Kaoru Aou, Shuhui Kang, and Shaw Ling Hsu*

Department of Polymer Science and Engineering and Materials Research Science and Engineering Center, University of Massachusetts Amherst, Amherst, Massachusetts 01003

Received May 18, 2005; Revised Manuscript Received June 29, 2005

ABSTRACT: Morphological features governing dimensional stability of variously processed poly(lactic acid) have been investigated. The exotherm observed near the glass transition temperature (T_g) is one of the most sensitive indicators reflecting structural changes as a function of temperature and time. A combination of spectroscopic and calorimetric techniques was used to analyze the amorphous chain conformation of deformed PLA samples. We found that nucleation-enhanced crystallization is the major contributor to the exotherm, not shrinkage. Our analysis suggests the existence of two amorphous regions. One is characteristic of the deformed structure. The other is consistent with a relaxed isotropic conformation distribution. Results showed that the existence of deformed amorphous chains is necessary for any fiber shrinkage. But above a critical crystallinity of 40%, a rigid crystalline network prevents shrinkage, even for highly deformed chains. In addition, the previously reported value of *tg′*t fraction in the amorphous region ($f_a = 0.80$) was validated in the current study.

Introduction

Poly(lactic acid) (PLA) attracts considerable interest from both fundamental and practical perspectives because it can be synthesized from renewable resources and is thus environmentally and economically appropriate. Since its degradation products are bioresorbable, this polymer is one of the select few appropriate for use in pharmaceutical applications.[1,2] The monomer is produced metabolically in two forms: L-lactic acid (with an S-stereocenter at the α-carbon) and D-lactic acid (R-stereocenter). The D-isomer can be obtained to different degrees depending on the selection of microbes in dextrose fermentation.[3] The L-isomer in high excess is easily obtained from fermentation, so that in practice PLA of high L-content is used. Varying the D/L ratio, i.e., the stereoisomer content in the backbone, has proven useful in controlling crystallization kinetics and maximum degree of crystallinity. Generally, PLA synthesis proceeds by ring-opening polymerization of the cyclic dimers of lactic acid that preserves the chirality at the α-carbon. The choice of dimers and appropriate catalyst makes available a wide range of PLA backbone sequences such as block,[4] alternating,[5] or simply random copolymers based on the same biomass-derived monomer.

Our previous studies focused on the chain conformation of PLA containing various amounts of the D-isomer.[6] Primarily on the basis of Raman spectroscopy and chain statistics analysis, it was established that PLA has a relatively rigid backbone with the most probable conformation being *tg′t* (present in 3/1 or 10/3 helix) along the lactyl backbone.[7,8] The notation *tg′t* refers to a trans planar ester C−O, gauche O−C_α, and trans C_α−C torsions, in that order. Those previous studies established through spectroscopy and simulation the relative population of the four conformers encountered in the PLA backbone: 80%, 10%, 5%, and 5% for *tg′t*, *tg′g*, *tt′t*, and *tt′g*, respectively. A high degree of crystallinity is achievable at a relatively small strain upon deformation of PLA chains. [9] In addition, the overall chain conformation distribution changes were characterized, revealing that conformational defects in the amorphous polymer chain are converted into more rigid and crystal-like *tg′t* conformations during deformation.[9] Spectroscopic and simulation analyses indicated that the presence of configurational defects increases chain flexibility[7] by destabilizing the *tg′t* conformational state at L−D junctions.[6] Conversely, a kinklike *tg′g* conformation becomes more stable. Therefore, an increased D-content in L-PLA results in less crystallization. At 15%D content ("%D"), the polymer was reported to be totally noncrystallizable.[10]

Our recent interest centers on the dimensional stability of various PLA product forms. Controllable dimensional stability of a polymeric material enhances its utility. Fibers usually require high stability, whereas films can be used as thermoforms and therefore require a varying level of structural stability for each specific application. Studies on the relationship between dimensional stability and structure have shown that shrinkage results from the presence of deformed amorphous chains and can be prevented by raising crystallinity levels.[11] Our previous study confirmed that a crystalline network indeed stabilizes PLA films.[12]

In differential scanning calorimetric measurements, oriented poly(ethylene terephthalate) (PET) showed an exotherm just above the glass transition temperature[13,14] that was interpreted as cold crystallization of oriented amorphous domains. Unlike melt-crystallization, there is no appreciable induction time before the observation of explosive crystallite growth. On the other hand, upon heating above T_g, drawn polystyrene (which are entirely amorphous) completely recovers applied strain and also exhibits an exotherm above T_g.[15] The exotherm observed above T_g (about 1.5 J g^{-1} for draw ratio of 9) was much smaller than observed for our PLA fibers and was attributed to mechanical shrinkage.[16,17] Those previous studies show that shrinkage and cold

* To whom correspondence should be sent: phone 413-577-1125; e-mail slhsu@polysci.umass.edu.

10.1021/ma051022e CCC: $30.25
Published on Web 08/04/2005

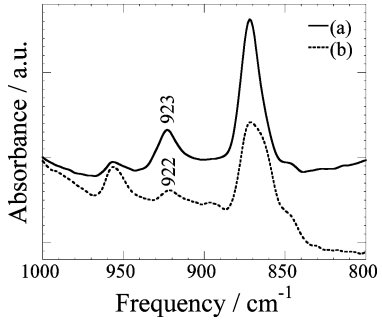

Figure 1. Infrared spectrum of (a) 4× drawn PLA film in transmission mode and (b) low-shrinkage PLA fiber, in ATR mode. In both cases, the incident radiation is polarized perpendicular to the orientation axis. For ATR, the plane of the ATR crystal is parallel to the polarization axis ("a.u." refers to arbitrary units).

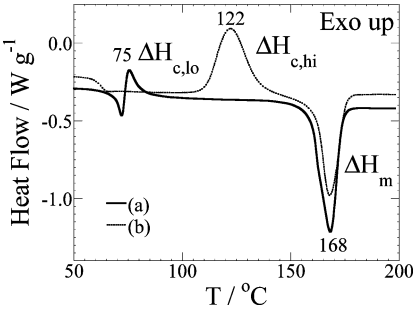

Figure 2. Thermograms of first and second heating of drawn 1.3%D film (for 10 °C min^{-1} heating rate): (a) first heating of drawn film; (b) second heating of drawn film after melting followed by quench-cooling in liquid nitrogen. Numbers label the peak temperatures in °C.

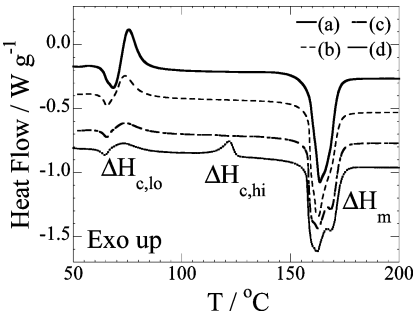

Figure 3. DSC thermograms of (a) high (>80%), (b) medium (~30%), (c) low-I (<20%, one exotherm), and (d) low-II (<20% two exotherms) shrinkage fibers.

crystallization are two events that can occur concurrently for deformed polymers.

Although many techniques are available for the characterization of crystalline phases, few are available to characterize the amorphous phase. Polymer structure at the molecular level can be probed using spectroscopic techniques. The conformer population distribution can be obtained by comparing experimental Raman spectral intensities to simulation studies.[7] The helical *tg′t* conformation is inherently abundant in amorphous PLA, so that the PLA backbone is expected to be rigid.[6,7] The combined use of spectroscopic and calorimetric methods for the evaluation of the molecular deformation of amorphous chains has been successful for PLA films. Our prior study shows that the deformation of amorphous PLA films increases the *tg′t* population, thereby facilitating strain-induced crystallization.[9] The present work uses the same spectroscopic technique on PLA fibers and relates the amorphous chain deformation to macroscopic thermal shrinkage. Differential scanning calorimetric data reveal two distinct types of amorphous regions in drawn PLA fibers. There are several studies on PLA fibers relating processing to property.[18−20] Our study addresses the connection between structural features of various deformed PLA samples and their dimensional stability.

Materials and Experimental Techniques

PLA melt-spun fiber and melt-extruded film samples with low D-content were received from Cargill Dow LLC (currently NatureWorks LLC). Samples of undrawn, extruded PLA films of various D-content were used in deformation studies. Since the melting enthalpy of a 100% PLA crystal is known only for the α-form, we needed to confirm that only α-crystals are present in our materials. Vibrational bands at 912 cm^{-1} for *β*-crystals and 923 cm^{-1} for α-crystals are assigned to CH_3 rocking coupled with O−C_α stretching.[8] As shown in Figure 1, on the basis of the spectroscopic features observed, these samples have predominantly crystals of the α-form.[21]

Thermal analyses were carried out using a TA Instruments model DSC2910A. Samples were heated at rates of 10, 20, 50, or 100 °C/min. For each heating rate, temperature was calibrated against the onset of melting of indium (156.6 °C). Heat flow was calibrated against the melting enthalpy of indium (28.5 J g^{-1}). Simple baseline procedure was used, and exothermic heat flow was integrated.

A Bruker model IFS88 Fourier transform Raman spectrometer was used to measure the orientation-independent Raman spectra. The 1064 nm line of the Nd:YAG laser was used for excitation. Spectral resolution was maintained at 4 cm^{-1}. To remove orientation effects and extract information on conformational distribution, fiber samples were mounted on a rotating stage with the rotation axis perpendicular to the fiber length and coincident with the laser path. Specific Raman-active vibrations that are sensitive to chain conformation have already been identified by previous simulation-based studies.[9]

A Perkin-Elmer Spectrum 2000 FT-IR spectrometer was used to obtain infrared spectra. Spectral resolution was also maintained at 4 cm^{-1}. Deformed PLA films were used with no further modification before measurement. For films too thick for measurement in the transmission mode, a KRS-5 crystal with an attenuated total reflectance (ATR) accessory setup was used to obtain reflection spectra.

A Jobin-Yvon Horiba LabRam-IR HR800 measured crystallinity in fibers and films to verify sample uniformity. The 632.8 nm line of a HeNe gas laser was used for excitation. Spectral resolution was ~4 cm^{-1} near the Rayleigh line. In this case, a CCD detector was used. Exact band positions were calibrated to silicon and polyethylene standards.

Results and Discussion

For various oriented PLA samples, two exothermic transitions were observed in two temperature ranges: one immediately above T_g for oriented samples ($\Delta H_{c,lo}$ Figure 2) and the other well above T_g for isotropic amorphous samples ($\Delta H_{c,hi}$, Figure 2). The origins of these transitions have not been defined. It is possible that the lower temperature transition and the higher temperature transition are associated with crystallization behavior of oriented and isotropic chains, respectively. These transitions suggest different types of amorphous structures. Oriented amorphous regions have been observed using atomic force microscopy.[19,20] All semicrystalline PLA fiber samples exhibiting shrinkage showed a $\Delta H_{c,lo}$ peak. Some fibers also displayed the additional $\Delta H_{c,hi}$ (Figure 3) peak, suggesting the existence of isotropic amorphous chains in addition to the oriented, dimensionally unstable amorphous chains. To illustrate the relationship between extent of shrinkage and $\Delta H_{c,lo}$, fiber samples were grouped into high

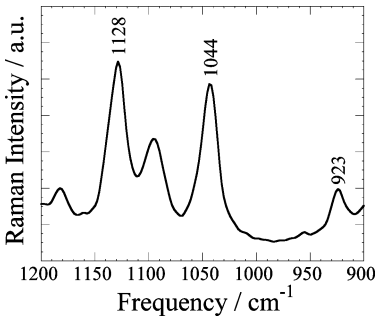

Figure 4. Raman spectrum of a melt-spun PLA fiber.

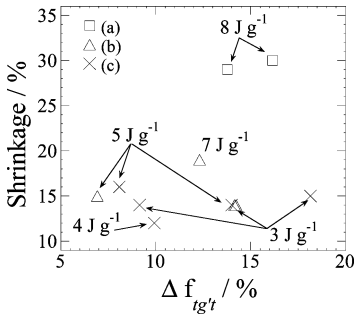

Figure 5. Shrinkage vs $\Delta f_{tg't}$ of low- to medium-shrinkage fibers, annotated with first exotherm values: (a) medium, (b) low-I, and (c) low-II shrinkage fibers.

(higher than 80%), medium (near 30%), low-I (shrinkage lower than 20% with only one exotherm), and low-II (likewise, with two exotherms) shrinkage fibers. Because the volumetric difference between amorphous and crystalline PLA is less than 3% (based on density values of 1256 and 1285 kg m^{-3}, respectively[22]), shrinkage values were not corrected for density effects. Crystals formed during DSC measurements as well as preexisting crystallites can be identified. The melting endotherm is usually observed to be bimodal in nature. Two distinguishable peaks with differing peak heat flow are observed. Fibers with lower shrinkage appear to have more area under the higher melting peak. This type of double melting peak has been previously attributed to melt recrystallization.[23,24]

Spectroscopic Analysis of Amorphous PLA Chains. Shrinkage data were compared with Raman spectroscopic results, namely with excess amorphous *tg′t* conformer population, $\Delta f_{tg't}$. For the purpose of computing $\Delta f_{tg't}$, we modified the theory outlined in a previous paper.[9] Previously, only structural modifications due to deformation and D-content were considered. Specifically, we used the equation (eq 6 in ref 9)

$$R = af_{tg't} + b \tag{1}$$

where R is the intensity ratio of the 1128 to 1044 cm^{-1} bands, as shown in Figure 4, and $f_{tg't}$ is the mole fraction of *tg′t* conformer in the PLA sample. The 1128 cm^{-1} peak is assigned to the methine C_α−H bending, and the 1044 cm^{-1} is assigned to CH_3 rocking coupled with methine C_α−H bending.[8] The values for (a, b) were found to be (−1.3, 2.4). These values were obtained from the calibration plot (Figure 7 in ref 9). We also added a modified equation from the same paper (eq 7 in ref 9):

$$f_{tg't} = X_C + f_a(1 - X_C) + \Delta f_{tg't} \tag{2}$$

where X_C is the degree of crystallinity, f_a is the equilibrium mole fraction of *tg′t* in the undeformed amorphous state (f_a = 0.80 for 0%D PLA[7]), and $\Delta f_{tg't}$ is the amount of *tg′t* in the amorphous in excess of the equilibrium value of 0.80. The quantity f_a is known from our spectroscopic studies to decrease with D-content. [6]

Semicrystalline polymers such as PLA do not deform affinely, especially for higher degrees of deformation. [9] Therefore, we sought to obtain the excess amorphous *tg′t* content from a molecular deformation parameter that can be computed from spectroscopic and calorimetric features. Thus, an equation expressing R as a function of X_C, X_D (mole fraction of D-lactyl residue in PLA backbone), and λ (molecular draw ratio) was introduced:

$$R(X_C,X_D,\lambda) = R_0 + \frac{\partial R}{\partial X_C}X_C + \frac{\partial R}{\partial X_D}X_D + \frac{\partial R}{\partial \lambda}(\lambda - 1) \tag{3}$$

From calibration studies, we find that the partial derivatives for X_C and X_D are constant for the respective variables ($\partial R/\partial X_C = -0.26$ and $\partial R/\partial X_D = 1.09$), and $R_0 = 1.37$. We also see a linear $\partial R/\partial\lambda$ for a noncrystallizable (13.0%D PLA). The changes in R as a function solely of λ, the molecular deformation, are as follows:

$$R_\lambda = -\frac{\partial R}{\partial \lambda}(\lambda - 1) \tag{4}$$

which then by substitution into eq 3 and rearrangement yields

$$R = 1.37 - 0.26X_C + 1.09X_D - R_\lambda \tag{5}$$

where R_λ is the decrease in R purely due to deformation. The boundary condition for eq 4 is $R_\lambda = 0$ for undeformed samples. We also note that, for the case where $X_C = 0$ and $\lambda = 1$ (undeformed amorphous polymer), eq 5 after substitution of eqs 1 and 2 becomes

$$f_a = 0.80 - 0.84X_D \tag{6}$$

which is in accordance with our previous simulation work, where we find that the *tg′t* conformation is destabilized and less favored at the D−L junctions.[6] Equations 1, 2, and 6, were then substituted into eq 5:

$$R_\lambda = 1.3\Delta f_{tg't} + 1.09X_CX_D \tag{7}$$

Our crystallinity was less than 45% for all samples, and the D-content of our PLA fibers were 2% so that the X_CX_D term is less than 0.01 and thus negligible. Then we get $\Delta f_{tg't}$ as a linear function of R_λ

$$\Delta f_{tg't} = 0.77R_\lambda \tag{8}$$

so that the excess in amorphous helical conformation can be obtained directly from spectroscopic measurements.

As shown in Figure 5, there are two scenarios for shrinkage: one where shrinkage is low for all values of $\Delta f_{tg't}$, and the second where shrinkage is proportional to $\Delta f_{tg't}$. In the first case, $\Delta H_{c,lo}$ values were all low in magnitude. In the second case, $\Delta H_{c,lo}$ values are directly proportional to $\Delta f_{tg't}$ and shrinkage. This figure also shows that an excess *tg′t* population beyond the unde-

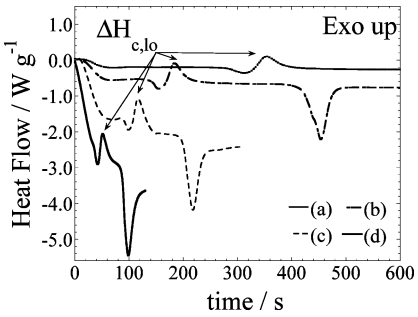

Figure 6. DSC thermograms of highly shrinkable fiber scanned at (a) 10, (b) 20, (c) 50, and (d) 100 °C min^{-1}.

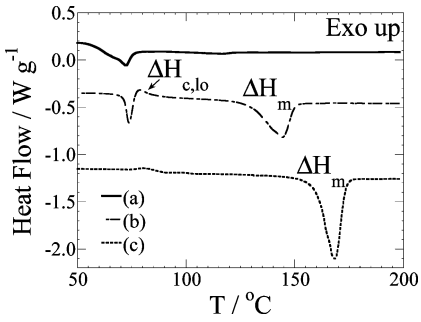

Figure 7. Thermograms of drawn films (a) 13.0%D, (b) 5.7%D, and (c) 1.3%D; 10 °C min^{-1} heating rate. 13.0%D film, a fully shrinkable film, does not exhibit any exotherm.

formed equilibrium amount does not guarantee high fiber shrinkage. That is, a finite $\Delta f_{tg't}$ is a necessary thermodynamic condition but not a sufficient kinetic condition for high shrinkage to occur. The kinetic barrier may be due to the presence of crystalline networks, as we previously reported for PLA films.[12] This is consistent with analysis for other semicrystalline polymers.[11]

It is worthwhile to consider morphological features associated with dimensional stability of PLA samples. The presence of deformed amorphous chains is a necessary condition in order for shrinkage to take place. An increase in entropy of deformed amorphous chains is the thermodynamic driving force for shrinkage. The presence of a crystalline network in a deformed sample is, however, sufficient for dimensional stability. This crystalline network serves as a kinetic barrier to dimensional change. Therefore, only a deformed amorphous chain combined with an absence of a crystalline network will lead to shrinkage.

Characterization of the First Post-T_g Exotherm. The degree of crystallinity is a required parameter for consideration of structural stability. A calorimetric determination of degree of crystallinity relies on the sum of the enthalpies of crystallization and melting. However, evidence exists relating dimensional stability and the presence of exothermic peaks. Therefore, the characterization of the identity of the physical event directly corresponding to the first post-T_g exotherm, i.e., whether it is crystallization, becomes a relevant problem.

An analysis of the magnitude of $\Delta H_{c,lo}$ on heating rate yields additional information concerning the nature of the phenomenon in question. For heating rates of 10, 20, 50, and 100 °C/min, the exotherms measured have values of 12 ± 2, 13.5 ± 0.9, 10.9 ± 0.1, and 9 ± 1 J g^{-1}, respectively. The first exotherm value does not change greatly with heating rate (Figure 6), indicating that the physical process corresponding to $\Delta H_{c,lo}$ happens very quickly, which can be either a conformational change associated with shrinkage or nucleation-enhanced crystallization.

To further characterize the post-T_g exothermic event, PLA films of differing D-contents were deformed and examined under DSC. These films, similar to the fiber samples, are uniaxially deformed and also exhibit shrinkage at temperatures above T_g. Isotropic and undeformed PLA films of low (1.3%D), medium (5.7%D), and high (13.0%D, noncrystallizable) D-contents were stretched to a draw ratio of six at 70 °C. The calorimetric data are presented in Figure 7. A draw ratio of six was chosen to achieve maximum deformation without brittle failure. After deformation, samples were quickly quenched into liquid nitrogen under tension. The endothermic dip near the glass transition, which represents sub-T_g physical aging of PLA,[25,26] did not affect our analysis. Figure 7 shows that the $\Delta H_{c,lo}$ peak appears only for the medium D-content film, whereas crystal melting (ΔH_m) appears for the low and medium D-content films. The 5.7%D and 13.0%D films were observed to shrink quickly back to their original dimensions at temperatures above T_g. The absence of a $\Delta H_{c,lo}$ peak does not necessarily indicate dimensional stability. Some possible reasons for drawn amorphous polystyrene exhibiting an exotherm is that the literature samples were drawn closer to its T_g (thus restricting stress relaxation and allowing efficient orientation) and that they were drawn to higher draw ratios. Since shrinkage is not the exothermic event in the case of PLA, the result from the heating rate dependence study suggests that the physical event is identified as nucleation-enhanced crystallization.

To support the previous point, one should recall Figure 2 which shows that the deformed sample has a more significantly depressed peak crystallization temperature (T_c) than the sample quenched from the melt. Even in the melt state, deformation is known to enhance nucleation.[27] The presence of nuclei and preexisting crystallites would then facilitate crystal growth at an early stage of heating. We therefore confirm that the identity of the physical event corresponding to $\Delta H_{c,lo}$ is thermal crystallization enhanced by strain-induced nucleation.[27]

Morphology Related to Dimensional Stability and Thermal Behavior. Morphological parameters no doubt control the extent of shrinkage in PLA. It has been suggested that in a deformed polymer a network of stable crystalline units is necessary to suppress shrinkage.[11,12] This network reduces the ability of deformed interconnected amorphous chains to shrink. In processing PET fibers, they are subjected to a heat setting process, i.e., annealed after deformation to increase sample crystallinity and therefore increased dimensional stability.[28,29] In the PLA fibers studied, shrinkage was not completely suppressed, as the fibers were intentionally not heat-set to allow a study of deformation effects. Interestingly for these PLA fibers, Figure 8 shows that the critical value lies in the region corresponding to a $\Delta H_{m,net}$ value that ranges from 34 to 39 J g^{-1}, which is about 37−42% crystallinity, using a previously determined value of 93 J g^{-1} for 100% α-crystalline PLA samples. [10] Above this value, samples exhibit considerable reduction in shrinkage.

We also have an interest in the factor affecting the extent of shrinkage upon reheating the fibers above T_g. The first crystallization exotherm ($\Delta H_{c,lo}$) value is very sensitive to the extent of shrinkage and is plotted

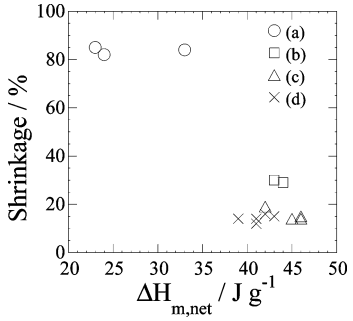

Figure 8. Shrinkage vs net melting enthalpy: (a) high, (b) medium, (c) low-I (one exotherm), and (d) low-II (two exotherms) shrinkage fibers.

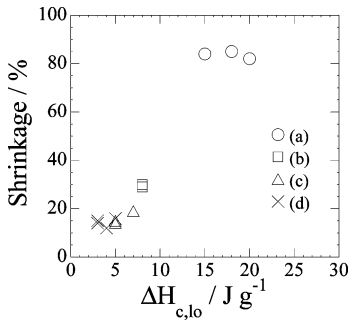

Figure 9. Shrinkage vs first post T_g exotherm (for 10 °C min^{-1} heating rate): (a) high, (b) medium, (c) low-I (one exotherm), and (d) low-II (two exotherms) shrinkage fibers.

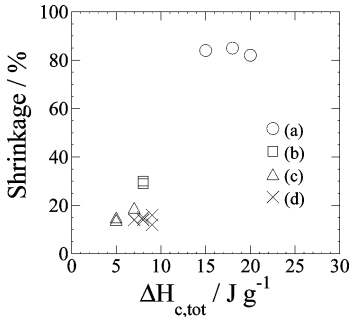

Figure 10. Shrinkage vs total exotherm (for 10 °C min^{-1} heating rate): (a) high, (b) medium, (c) low-I (one exotherm), and (d) low-II (two exotherms) shrinkage fibers.

against shrinkage in Figure 9. There is a simple, monotonic relationship between shrinkage and exotherm, as the low, medium, and high shrinkage fibers are clearly differentiated just by comparing the exotherms observed. Shrinkage, although exothermic by nature, does not generate the exotherm in question. The correlation between mechanical shrinkage and exothermic heat flow can therefore be only indirectly causal. Our present work indicates that the exotherm is caused by nucleation-enhanced thermal crystallization. Correlation between shrinkage and crystallization exotherm would then suggest that the shrinkable amorphous chains are also deformed chains that did not crystallize during the deformation process. The amount of deformed crystallizable amorphous chains, represented quantitatively by $\Delta H_{c,lo}$, directly corresponds to the extent of shrinkage possible upon reheating.

The relationship between shrinkage and the sum of all crystallization exotherms ($\Delta H_{c,tot}$) is shown in Figure 10. A general trend is observed that high shrinkage fibers (shrinkage >80%) crystallize more. This relationship cannot be used to differentiate the fine differences

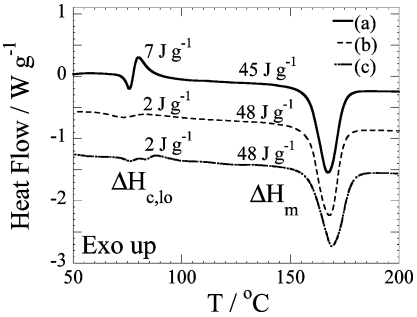

Figure 11. DSC thermograms of shrinkable PLA film: (a) as-is, (b) heated free-ended, and (c) heated under strain. Heating rate of 20 °C min^{-1} was used. The thermal history of the films after deformation and before DSC was heating at 82 °C for 1 min.

between low-I (shrinkage < 20%, one exotherm), low-II (shrinkage < 20%, two exotherms), and medium shrinkage (shrinkage ~ 30%) fibers. This results from the fact that $\Delta H_{c,tot}$ includes contributions from $\Delta H_{c,hi}$ (Figures 2 and 3) which represents crystallization of relaxed amorphous chains and is unrelated to shrinkage. This also further confirms that $\Delta H_{c,lo}$ represents an amount of deformed amorphous chains, the molecular origin for why $\Delta H_{c,lo}$ and fiber shrinkage coincide.

In general, it is well established that deformation of a polymer gives rise to enhanced crystal nucleation.[27] This is explained as a rise in equilibrium melting temperature due to the conformational entropy drop resulting from the applied deformation.[30] In this study, we conclude that the first exotherm ($\Delta H_{c,lo}$) upon reheating represents nucleation-enhanced thermal crystallization. The effect of orientation in chains on crystal growth during secondary crystallization is of substantial interest. For this study, a shrinkable semicrystalline 1.3%D PLA film was used. Two types of samples were prepared: (i) heated at 82 °C for 1 min with one end free ("relaxed sample"); (ii) heated 82 °C for 1 min, under strain with both ends fixed ("strained sample"). The temperature was chosen to coincide with the peak of the post-T_g exotherm for shrinkable fibers. This comparison was designed to show any effects of amorphous deformation on subsequent crystallization. The result, as presented in Figure 11, shows no discernible differences between the two samples. Strained samples with oriented chains did not have enhanced crystal growth in comparison with the free-ended samples with previously oriented but subsequently relaxed chains. These analyses on PLA showed that although applied deformation affected strain-induced nucleation and crystallization, residual amorphous orientation did not affect crystal growth upon reheating.

Conclusions

This study illustrated the existence of a critical degree of crystallinity beyond which fiber shrinkage is suppressed. This critical degree is ~40%. We also established a technique to analyze the excess helical conformation in the amorphous chains. Using this technique, we confirmed that the presence of deformed amorphous chains is the thermodynamic driving force for shrinkage, but a presence of critical crystallinity suppressed shrinkage. A series of calorimetric studies demonstrated that deformed amorphous chains are detectable through the presence of a post-T_g crystallization exotherm. Calorimetric studies also suggested that post-T_g crystallization is nucleation-enhanced. These studies further indicated

the existence of two amorphous chain types: deformed and relaxed. Amorphous chain orientation did not have an effect on crystal growth of fibers during reheating.

Acknowledgment. The authors thank the National Science Foundation-Environment Protection Agency (TSE Grant RD831636010) and the Materials Research Science and Engineering Center at University of Massachusetts for their financial support. We also appreciate a grant from the National Science Foundation, Materials Research Science and Engineering Center for supporting this research.

References and Notes

(1) Jain, R.; Shah, N. H.; Malick, A. W.; Rhodes, C. T. *Drug Dev. Ind. Pharm.* **1998**, *24*, 703−727.
(2) Jain, R. A. *Biomaterials* **2000**, *21*, 2475−2490.
(3) Manome, A.; Okada, S.; Uchimura, T.; Komagata, K. *J. Gen. Appl. Microbiol.* **1998**, *44*, 371−374.
(4) Nomura, N.; Ishii, R.; Akakura, M.; Aoi, K. *J. Am. Chem. Soc.* **2002**, *124*, 5938−5939.
(5) Chamberlain, B. M.; Cheng, M.; Moore, D. R.; Ovitt, T. M.; Lobkovsky, E. B.; Coates, G. W. *J. Am. Chem. Soc.* **2001**, *123*, 3229−3238.
(6) Kang, S. H.; Zhang, G. Z.; Aou, K.; Hsu, S. L.; Stidham, H. D.; Yang, X. Z. *J. Chem. Phys.* **2003**, *118*, 3430−3436.
(7) Yang, X. Z.; Kang, S. H.; Hsu, S. L.; Stidham, H. D.; Smith, P. B.; Leugers, A. *Macromolecules* **2001**, *34*, 5037−5041.
(8) Kang, S. H.; Hsu, S. L.; Stidham, H. D.; Smith, P. B.; Leugers, M. A.; Yang, X. Z. *Macromolecules* **2001**, *34*, 4542−4548.
(9) Yang, X. Z.; Kang, S. H.; Yang, Y. N.; Aou, K.; Hsu, S. L. *Polymer* **2004**, *45*, 4241−4248.
(10) Fischer, E. W.; Sterzel, H. J.; Wegner, G. *Kolloid Z. Z. Polym.* **1973**, *251*, 980−990.
(11) Trznadel, M.; Kryszewski, M. *J. Macromol. Sci., Rev. Macromol. Chem. Phys.* **1992**, *C32*, 259−300.
(12) Smith, P. B.; Leugers, A.; Kang, S. H.; Hsu, S. L.; Yang, X. Z. *J. Appl. Polym. Sci.* **2001**, *82*, 2497−2505.
(13) Mascia, L.; Fekkai, Z. *Polymer* **1993**, *34*, 1418−1422.
(14) Gupta, V. B.; Radhakrishnan, J.; Sett, S. K. *Polymer* **1993**, *34*, 3814−3822.
(15) Hadziioannou, G.; Wang, L. H.; Stein, R. S.; Porter, R. S. *Macromolecules* **1982**, *15*, 880−882.
(16) Rogers, M. G. *J. Mater. Sci.* **1991**, *26*, 4285−4287.
(17) Sun, D. C.; Magill, J. H. *Polym. Eng. Sci.* **1989**, *29*, 1503−1510.
(18) Mezghani, K.; Spruiell, J. E. *J. Polym. Sci., Polym. Phys.* **1998**, *36*, 1005−1012.
(19) Cicero, J. A.; Dorgan, J. R.; Janzen, J.; Garrett, J.; Runt, J.; Lin, J. S. *J. Appl. Polym. Sci.* **2002**, *86*, 2828−2838.
(20) Cicero, J. A.; Dorgan, J. R.; Garrett, J.; Runt, J.; Lin, J. S. *J. Appl. Polym. Sci.* **2002**, *86*, 2839−2846.
(21) Sawai, D.; Takahashi, K.; Imamura, T.; Nakamura, K.; Kanamoto, T.; Hyon, S. H. *J. Polym. Sci., Polym. Phys.* **2002**, *40*, 95−104.
(22) Miyata, T.; Masuko, T. *Polymer* **1998**, *39*, 5515−5521.
(23) Wunderlich, B. *Macromolecular Physics*; Academic Press: New York, 1980; Vol. 3.
(24) Yasuniwa, M.; Tsubakihara, S.; Sugimoto, Y.; Nakafuku, C. *J. Polym. Sci., Polym. Phys.* **2004**, *42*, 25−32.
(25) Celli, A.; Scandola, M. *Polymer* **1992**, *33*, 2699−2703.
(26) Liao, K. R.; Quan, D. P.; Lu, Z. J. *Eur. Polym. J.* **2002**, *38*, 157−162.
(27) Wunderlich, B. *Macromolecular Physics*; Academic Press: New York, 1976; Vol. 2.
(28) Gupta, V. B.; Kumar, S. *J. Appl. Polym. Sci.* **1981**, *26*, 1865−1876.
(29) Gupta, V. B. *J. Appl. Polym. Sci.* **2002**, *83*, 586−609.
(30) Flory, P. J. *J. Chem. Phys.* **1947**, *15*, 397−408.

MA051022E